EINDHOVEN UNIVERSITY OF TECHNOLOGY

Surface roughness in XeF2 etching of a-Si/c-Si(100)

Citation for published version (APA):
Stevens, A. A. E., & Beijerinck, H. C. W. (2005). Surface roughness in XeF2 etching of a-Si/c-Si(100). *Journal of Vacuum Science and Technology A*, *23*(1), 126-136. https://doi.org/10.1116/1.1830499

DOI:
10.1116/1.1830499

Document status and date:
Published: 01/01/2005

Document Version:
Publisher's PDF, also known as Version of Record (includes final page, issue and volume numbers)

Please check the document version of this publication:

• A submitted manuscript is the version of the article upon submission and before peer-review. There can be important differences between the submitted version and the official published version of record. People interested in the research are advised to contact the author for the final version of the publication, or visit the DOI to the publisher's website.
• The final author version and the galley proof are versions of the publication after peer review.
• The final published version features the final layout of the paper including the volume, issue and page numbers.

Link to publication

General rights
Copyright and moral rights for the publications made accessible in the public portal are retained by the authors and/or other copyright owners and it is a condition of accessing publications that users recognise and abide by the legal requirements associated with these rights.

• Users may download and print one copy of any publication from the public portal for the purpose of private study or research.
• You may not further distribute the material or use it for any profit-making activity or commercial gain
• You may freely distribute the URL identifying the publication in the public portal.

If the publication is distributed under the terms of Article 25fa of the Dutch Copyright Act, indicated by the "Taverne" license above, please follow below link for the End User Agreement:

www.tue.nl/taverne

Take down policy
If you believe that this document breaches copyright please contact us at:

openaccess@tue.nl

providing details and we will investigate your claim.

Download date: 16. Nov. 2023

Surface roughness in XeF_2 etching of *a*-Si/*c*-Si(100)

A. A. E. Stevens[a] and H. C. W. Beijerinck
Physics Department, Eindhoven University of Technology, P.O. Box 513, 5600 MB Eindhoven, The Netherlands

(Received 27 July 2004; accepted 18 October 2004; published 15 December 2004)

Single wavelength ellipsometry and atomic force microscopy (AFM) have been applied in a well-calibrated beam-etching experiment to characterize the dynamics of surface roughening induced by chemical etching of a ~12 nm amorphous silicon (*a*-Si) top layer and the underlying crystalline silicon (*c*-Si) bulk. In both the initial and final phase of etching, where either only *a*-Si or only *c*-Si is exposed to the XeF_2 flux, we observe a similar evolution of the surface roughness as a function of the XeF_2 dose proportional to $D(XeF_2)^\beta$ with $\beta \approx 0.2$. In the transition region from the pure amorphous to the pure crystalline silicon layer, we observe a strong anomalous increase of the surface roughness proportional to $D(XeF_2)^\beta$ with $\beta \approx 1.5$. Not only the growth rate of the roughness increases sharply in this phase, also the surface morphology temporarily changes to a structure that suggests a cusplike shape. Both features suggest that the remaining *a*-Si patches on the surface act effectively as a capping layer which causes the growth of deep trenches in the *c*-Si. The ellipsometry data on the roughness are corroborated by the AFM results, by equating the thickness of the rough layer to 6 σ, with σ the root-mean-square variation of the AFM's distribution function of height differences. In the AFM data, the anomalous behavior is reflected in a too small value of σ which again suggests narrow and deep surface features that cannot be tracked by the AFM tip. The final phase morphology is characterized by an effective increase in surface area by a factor of two, as derived from a simple bilayer model of the reaction layer, using the experimental etch rate as input. We obtain a local reaction layer thickness of 1.5 monolayer consistent with the 1.7 ML value of Lo *et al.* [Lo *et al.*, Phys. Rev. B **47**, 648 (1993)] that is also independent of surface roughness. © *2005 American Vacuum Society.* [DOI: 10.1116/1.1830499]

I. INTRODUCTION

Plasma etching is the standard etching technique in the production of integrated circuits, MEMS devices, and photonic devices. The main advantage of plasma etching is the directionality that is imposed by the ions that bombard the surface of the device.[1] However, the etch process gives rise to surface roughness depending on the various plasma parameters, such as ion energy and ion-to-etchant flux ratio. As device dimensions continue to shrink, any roughness, caused by the device production process, plays a key role in eventual device performance.

In optimizing plasma etch processes, the main problem one comes across is the tremendous complexity of the plasma environment. This makes it exceedingly difficult to get an understanding of the reaction mechanisms involved. To circumvent the difficulties associated with plasma etching, many experiments have been performed[2] that give a picture of the processes involved. In several beam etching systems, fairly complete and accurate models have been developed. The present system has also been studied intensively by etch product analysis.[3–12] However, surface roughness caused by the etching has never been characterized in detail, although various authors[2,7,13] mention the importance in fully understanding the obtained models inspired by etch product analysis.

Ellipsometry is by far the most commonly used *in situ* surface diagnostic to look at the surface roughness. Therefore, ellipsometry is applied to a beam etching experiment to characterize the surface roughness. The fact that ions and etchant can be manipulated independently helps in revealing the role of ions and etchant in the roughening process on a more fundamental level. Aliev *et al.*[14] looked into the initial stage of *c*-Si surface roughening caused by XeF_2 etching with ellipsometry. This work will report on the roughness caused by XeF_2 etching of an amorphous silicon (*a*-Si) layer and subsequently the underlying crystalline silicon [*c*-Si(100)] sample. The *a*-Si layer is produced by 2.5 keV Ar^+ ion bombardment. The amorphization of *c*-Si has been studied quite intensively in terms of roughness, damage profiling, and simulations by Refs. 15–21 and many others, although most studies are done by surface probe measurements, such as atomic force microscopy (AFM) and scanning tunneling microscopy (STM), and for ion energy ranges other than 0.5–2.5 keV as presented here. In Sec. III the ellipsometric characterization of the *a*-Si layer will be addressed and also the surface roughness caused by the impinging ions. This information is required in Sec. IV, addressing the subsequent chemical XeF_2 etching of the *a*-Si layer and the underlying *c*-Si sample. A comparison will be made between the roughness determined with *in situ* ellipsometry and the roughness of samples which have been analyzed *ex situ* with atomic force microscopy (AFM). The surface roughness caused by the XeF_2 etching affects the interpretation of the existing reaction layer models for XeF_2 etching of

[a]Electronic mail: a.a.e.stevens@tue.nl

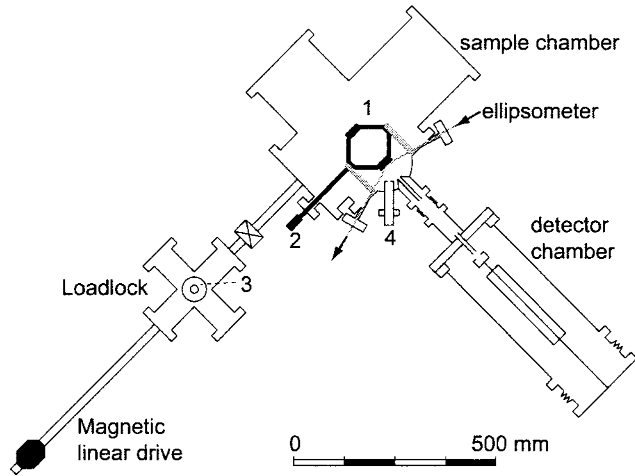

FIG. 1. Revised setup in horizontal cross section. The sample is mounted in a rotatable sample holder (1) that can be operated manually via an external drive (2). Samples can be exchanged between the sample holder and the sample storage (3) in the load lock with a linear magnetic drive. The ion gun and the XeF_2 source (4) are at 45° and 52° from surface normal, respectively. The ellipsometer is at 74° from the sample surface normal. Etch products are detected in a separate detector chamber perpendicular to the sample surface.

silicon deduced from product analysis. A discussion based on the bilayer model[7,13] will address the issue of silicon-fluoride reaction layer thickness in Sec. V. The gathered information from ellipsometry and AFM can be used to obtain a geometrical picture of the rough surface. Some characteristic measures of the rough surface are described in Sec. VI. Finally, some conclusions are made in Sec. VII.

II. EXPERIMENTAL DETAILS

The setup used has been described extensively in earlier publications.[3,4] In this section only the two modifications that have been made recently will be discussed. These are the addition of a sample exchange mechanism and the addition of an ellipsometer. A brief description of ellipsometry and measurement interpretation will also be given.

A. Vacuum apparatus

A schematic view of the setup and relative orientation of the beams onto the sample is shown in Fig. 1. The sample holder has been replaced by a rotatable two-slot sample holder. This sample holder has two slots in order to enable the calibration of the mass spectrometer. In the standard position of the sample holder, the sample surface is oriented toward the multiple-beam setup. The sample can be rotated to be in the path of a magnetic linear drive in the vacuum. With this linear drive, the sample can be transported to the load lock. The load lock has a capacity of six samples and a base pressure of 1×10^{-8} mbar, achieved by a turbomolecular pump of 56 l/s. A valve separates the loadlock from the main chamber. The sample chamber has a base pressure of 1×10^{-8} mbar and is pumped by turbomolecular pumps. All fluxes impinging on the sample are measured in monolayers per second (ML/s); one monolayer corresponds to 6.86×10^{18} m^{-2}, the surface density of Si(100). The Ar^+ ion flux can be varied from 0 to 0.11 ML/s and the ion energy ranges from 0.5 to 2.5 keV. The ion beam impinges at a 45° angle of incidence. The XeF_2 flux can be varied from 0 to 3.6 ML/s and impinges at a 52° angle of incidence.

B. Ellipsometry

This section gives a brief outline of ellipsometry. A full theory can be found in the book by Azzam and Bashara.[22] Ellipsometry is a surface diagnostic that uses the change in ellipticity that a light beam undergoes during reflection at a surface. The Fresnel equations require that reflection coefficients for polarization parallel (R_p) and perpendicular (R_s) to the plane of incidence differ. This is usually expressed as a reflectance ratio ρ:

$$\rho=\frac{R_p}{R_s}=\tan(\Psi)\times e^{i\Delta}. \tag{1}$$

Equation (1) defines the ellipsometric angles Ψ and Δ. The factor $\tan\Psi$ is the ratio of the reflected amplitudes of the p and s waves. The phase difference between the reflected p and s waves is called Δ. Both angles are traditionally expressed in degrees.

The reflectance ratio ρ that is measured depends on the refractive index and the morphology of the surface under investigation, as well as on the wavelength used, the angle of incidence, and the presence of thin films on the surface. A medium consisting of a mixture of two different substances (labeled 1 and 2) is modeled as an *effective medium*. The dielectric constant ϵ_r of the effective medium is found by solving the Bruggemann equation[23]

$$0=\nu_1\frac{\epsilon_{r,1}-\epsilon_r}{\epsilon_{r,1}+2\epsilon_r}+\nu_2\frac{\epsilon_{r,2}-\epsilon_r}{\epsilon_{r,2}+2\epsilon_r}. \tag{2}$$

Here the (complex) dielectric constants of media 1 and 2 are called $\epsilon_{r,1}$ and $\epsilon_{r,2}$, respectively. Medium i ($i=1,2$) occupies a volume fraction ν_i, with $\Sigma_i\nu_i=1$. The complex refractive index of a medium is given by $\epsilon=\tilde{n}^2$. In the case of a rough top layer, one of the media is vacuum with $\epsilon_r=1$.

The interpretation of the measured Ψ and Δ is quite cumbersome. The Fresnel equations have no easy proportionalities in them. In the case of a substrate with a film on top, all internal reflections in the film have to be taken into account, further complicating matters. This is why the interpretation of the data measured is done by comparison with computer simulations. For this work, a computer program based on the impedance algorithm[24] was used. This allows the interpretation of measurements on substrates that have several thin layers stacked on top of one another. The refractive indices used in the analysis of these measurements are given in Table I.

C. Rotating-compensator ellipsometer

The setup for the ellipsometry is a rotating-compensator ellipsometer in the polarizer-compensator-sample-analyzer configuration. The laser light used is linearly polarized

TABLE I. Numerical values of the refractive indices for the various layers assumed for data analysis and for reference.

Used for	Material	Assumed $\tilde{n}$
Modeling	Crystalline silicon (*c*-Si)	3.88–0.02 *j*[a]
	SiO_2	1.46[b]
	Amorphized silicon (*a*-Si)	4.58−*i*0.72[c]
Reference	Amorphized silicon (*a*-Si)	4.63−*i*0.76[d]
	Rough SiF_x	1.6[e]
	SiCl	1.66[f]

[a]Reference 32.
[b]Reference 33.
[c]Reference 26.
[d]Reference 15.
[e]Reference 29.
[f]Reference 30.

632.8 nm light from a He–Ne laser. The angle of incidence onto the sample was chosen to be around 74° for maximum sensitivity on silicon. The light is made circular with a $\lambda/4$ retarder. The polarizer and analyzer used are dichroic sheet polarizers with an extinction coefficient of 10^4. They can both be manually adjusted to within 0.05° of the desired settings. The rotating compensator is driven by a synchronous motor at line frequency, with a 2:3 transmission in between for noise suppression, rotating at 33 Hz. An encoding system gives off trigger pulses at every $2\pi/256$ radians. The compensator itself is a zero-order $\lambda/4$ retarder, with a double antireflective coating ($R<0.05\%$). The polarizing properties of the compensator are also expressed in terms of ellipsometric angles Ψ and Δ. The light beam enters and leaves the vacuum through stress-free, nonpolarizing quartz windows. The reflected light is detected by a photodiode, and amplified. Then the detected signal is fed into a 12-bit parallel sampling analog-to-digital converter (ADC) (resolution 2.44 mV). The ADC is read at every trigger pulse. The resulting signal is Fourier-analyzed in real time by a computer. The resulting values of Ψ and Δ are extracted from the Fourier coefficients. Furthermore, the computer program used for the measurements allowed synchronously monitoring various chemical species coming from the sample by the mass spectrometer. In Sec. II D a brief description of the product flux calibration is given.

Before each insertion into the vacuum system the *n*-type Si(100) samples ($\rho=10-30\ \Omega$ cm) are cleaned with alcohol, leaving the native oxide layer in place. All measurements presented here are performed at room temperature. Prior to a series of measurements, the plane of incidence onto the sample was calibrated using the native oxide layer, as done by Smets *et al.*[25] Subsequently, the compensator is calibrated. Again, the native oxide layer serves its purpose by allowing the determination of the angle of incidence of the laser beam on the sample. The native oxide layer is found to be 2.2±0.3 nm thick from sample to sample. The angle of incidence is found to vary between 73.95° and 74.15°, since each sample is inserted into the sample holder in a slightly different position. Rotating the sample back and forth for product flux calibration resulted in variations of less than 0.05° in the angle of incidence.

D. Product flux calibration

To calibrate the pulse counting system of the mass spectrometer to absolute values of the flux leaving the sample an inert Ni sample is used, which does not interact with XeF_2. For this purpose the sample holder is rotated such that a Ni sample is in the focus of the beams and the detector acceptance. The XeF^+ count rate is calibrated with the absolute value of the impinging XeF_2 flux of 0.9 ML s^{-1} ($=6.2\times10^{14}$ cm^{-2} s^{-1}). Rotating the Si sample back into position, the loss of XeF_2 flux due to etching (as visible in the loss of XeF^+ count rate) is equal to the SiF_4 flux leaving the sample, because SiF_4 is known to be the only etch product at room temperature.[3] This absolute flux is used to calibrate the SiF_3^+ count rate which is used as a fingerprint of SiF_4. Now, the mass spectrometer count rates directly represent an absolute flux of reagents and products, an essential condition for understanding etch dynamics. The etch rate is now expressed in the production coefficient δ defined as

$$\delta=\frac{2\Phi(SiF_4)}{\Phi_s(XeF_2)} \quad (3)$$

with $\Phi_s(XeF_2)$ the impinging flux on the sample and $\Phi(SiF_4)$ the product flux leaving the sample. The production coefficient or etching efficiency is defined such that $\delta=1$ corresponds to the full conversion of reactant into products. The etch rate of silicon at the sample is given by

$$\frac{d[\mathrm{Si}]}{dt}=\frac{\delta}{2}\Phi_s(XeF_2), \quad (4)$$

which reflects that we need two reactant molecules to form a product molecule. By inserting the thickness $a_{Si}=0.138$ nm/ML of a monolayer of Si, the Si etch yield Y_{Si} (nm) is related to the total dose $D(XeF_2)$ (ML) of reactant delivered to the surface, as given by

$$Y_{Si}=a_{Si}\frac{\delta}{2}D(XeF_2). \quad (5)$$

This relation allows tracking of the total amount of Si removed during our experiments. Further details concerning the mass spectrometer and the product analysis have been reported in the past.[3,4,7]

III. AMORPHIZATION OF c-Si

The production of the amorphized (*a*-Si) layer by Ar^+ ions will be described briefly, since ellipsometry has never been performed on Ar^+ sputtering with ion energies in the range of 1.0–2.5 keV. Furthermore, this information is required to described the XeF_2 etching in the following section. A more elaborate treatise will be published elsewhere.[26]

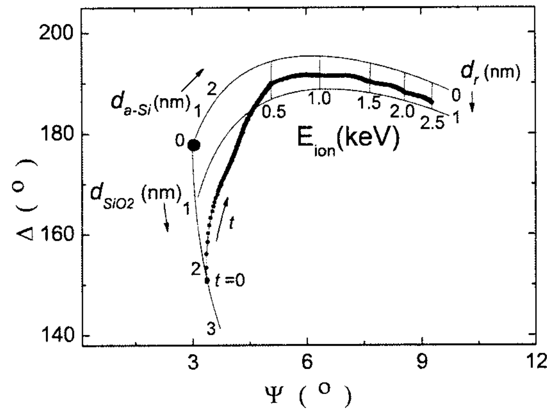

FIG. 2. Ψ,Δ-plot of a measurement of Ar^+ sputter etching (connected dots). The drawn lines are simulations on the basis of Fig. 3. The large dot represents (Ψ,Δ) for a clean *c*-Si sample. At $t=0$ the *c*-Si is covered by a 2.1 nm native oxide layer. When Ar^+ ions are switched on steady state (Ψ,Δ) situations are reached for the various ion energies. A corresponding amorphized layer thickness $d_{a\text{-Si}}$ and a rough layer thickness d_r is found by matching the simulations to the measurement.

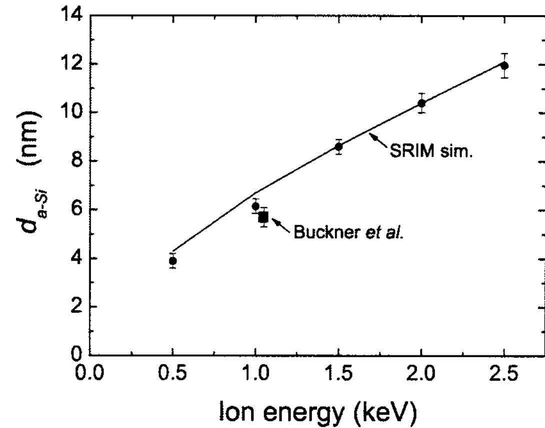

FIG. 4. *a*-Si thickness as a function of Ar^+ ion energy (●) including SRIM simulations (straight line) and a result obtained by Buckner *et al.* (Ref. 16) (■).

A. Model

In Fig. 2 an ellipsometry measurement of the Ar^+ etching of *c*-Si is shown (connected dots). The large dot represents the model values of Ψ and Δ of a clean *c*-Si sample, i.e., no native-oxide layer, roughness or amorphized Si layer. At $t=0$ the *c*-Si sample is covered by a thin native oxide layer. By matching the simulation of an increasing native oxide layer thickness on top of a *c*-Si bulk layer [Fig. 3(a)] to the measured Ψ and Δ the native oxide layer thickness is obtained. In this case the native-oxide layer thickness is found to be 2.1 nm. The refractive indices required for the simulations are listed in Table I.

Next, Ar^+ ions with an energy of 0.5 keV and a flux of 0.011 ML s^{-1} ($=7.5\times10^{12}$ cm^{-2} s^{-1}) are switched on resulting in an increase of Ψ and Δ. The ions initially remove the native-oxide layer. Simultaneously the ions generate an *a*-Si layer with a rough layer on top, eventually going to a steady state values of Ψ and Δ. Subsequently the ion energy is increased with steps of 0.5 keV up to 2.5 keV keeping the ion flux constant. The ellipsometric parameter Ψ increases with increasing ion energy whereas little variation can be observed for Δ. At each energy a steady state situation is reached.

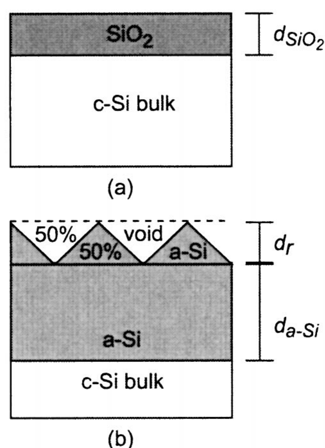

FIG. 3. Layer models used in the ellipsometry simulations for (a) the bare sample with a native oxide film on top and for (b) the Ar^+ ion sputter etching. The model for the Ar^+ ion sputter simulation consists of an *a*-Si layer and a rough layer on top, which is a mixture of 50% void and 50% *a*-Si.

Next, a multilayer model is required to obtain *a*-Si layer thickness $d_{a\text{-Si}}$ and rough layer thickness d_r in which the rough layer is constituted from 50% void and 50% *a*-Si via the Bruggemann equation Eq. (2). The complex refractive index used for *a*-Si is mentioned in Table I and has been determined in a more extensive study.[26] Note that the values for n and k used here are in good agreement with the values reported by Fried *et al.*[15] (See Table I), although they used 20 keV Ar^+ ions to amorphise a Si sample. The simplest model to describe the measurement is shown in [Fig. 3(b)]. Two simulations by means of this model are shown in Fig. 2. Both simulations result from increasing the *a*-Si layer from 0 to 15 nm keeping the rough layer thickness constant at 0 and 1 nm, respectively. The following sections will show that this multilayer model gives a good description of the Ar^+ etching of *c*-Si.

B. *a*-Si layer thickness

The *a*-Si layer thickness is determined by matching measurement and simulation at the steady state Ψ and Δ for each ion energy. The resulting *a*-Si layer thickness as a function of ion energy is shown in Fig. 4. The errors are derived from ten measurements on ten different samples. The *a*-Si layer thickness for 1.05 keV Ar^+ ions determined by Buckner *et al.*[16] is also included. Buckner used the complex refractive index determined by Fried *et al.*[15] (Table I). The difference between his result and ours is an indication of the difference in *a*-Si layer thickness resulting from the difference in complex refractive index.

With increasing ion energy the *a*-Si layer thickness increases, because the ions penetrate deeper into the silicon sample. Note that the *a*-Si layer thickness is in fact an effec-

tive layer thickness, since the amorphous to crystalline transition is not discrete but gradual.[18] A comparison with, e.g., (SRIM)[17] is therefore not straightforward. Here, a comparison is made by looking at the distribution of vacancy-causing collisions (vacancies/nm/ion) as a function of depth. The solid line in Fig. 4 represents the depth in SRIM that corresponds to a level of vacancy-causing collisions equal to 0.1 vacancy/nm/ion, which is in good agreement with the measured effective *a*-Si layer thickness. These conditions clearly define the depth of the effective discrete transition from *a*-Si to *c*-Si.

C. Roughness

The rough layer is simulated using the Bruggemann effective medium approximation [Eq. (2)] using a mixture of 50% voids and 50% *a*-Si. The rough layer thickness is on the order of 0.65 ± 0.05 nm and shows no clear dependence on the ion energy. A similar degree of roughness caused by ion etching was reported by various authors not only on Si[19–21] but also on other materials.[27,28] The minor differences can be easily related to the difference in diagnostic tool or experimental conditions such as ion angle of impingement, ion flux, ion dose, and ion energy differences. Note that here the ions are still switched on when the roughness is determined. Surface probe measurements (AFM/STM) afterward might give a different roughness due to surface relaxation once the ions are switched off. More importantly, surface probe measurements give a different measure for surface roughness (root-mean-square roughness σ) than the rough layer thickness from ellipsometry which makes a quantitative comparison not straightforward.

The rather low roughness result can be explained by surface smoothing.[27] After impact of the energetically incident ions, a heat spike of 1 ps melts the surface locally, allowing the surface to relax. One would expect this surface smoothing process, thus also the surface roughness, to be ion energy dependent. Here, the surface roughness shows no clear dependence on the incident ion energy. The energy deposited at the surface by the impinging ions with energies between 0.5 and 2.5 keV results in a lowering of the binding energy of surface atoms and consequently in an improvement of the sputter yield. A higher sputter yield may lead to a higher roughness. But simultaneously more energy is available for surface relaxation. Apparently, the two effects cancel out. Hence, a pronounced ion energy dependence of the surface roughness is not observed.

To conclude, the ion damage layer thickness and surface roughness obtained with ellipsometry can be explained and the results are in good agreement with literature. This insight in the amorphization process provides the necessary information to study the chemical XeF_2 etching of a 2.5 keV Ar^+ created, 12 nm *a*-Si layer and subsequently the underlying *c*-Si bulk.

IV. CHEMICAL XeF_2 ETCHING

In this section the ellipsometric characterization of the XeF_2 etching of a 12 nm *a*-Si layer and the underlying *c*-Si bulk sample will be addressed. The different models used to analyze the ellipsometry data are discussed, elaborating on the approximations made. The evolution of the roughness in time will be compared to AFM measurements and the amorphous-to-crystalline transition region will be discussed in detail.

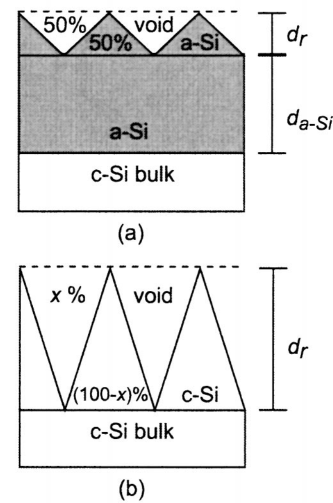

FIG. 5. Layer models used in the ellipsometry simulations for (a) short term and for (b) long term XeF_2 etching.

A. Model

To obtain the surface roughness, again (multi-)layer models describing the surface are required. The used models are shown in Fig. 5. In time, the *a*-Si layer will be etched away and in the process the roughness increases [Fig. 5(a)]. When the *a*-Si layer is completely removed, the etching continues on the underlying bulk *c*-Si [Fig. 5(b)]. In general, a ratio of 50% void/50% material is used to model the roughness. Here, the percentage void x is used as an additional fit parameter.

These models lack the presence of a SiF reaction layer contribution. The question therefore is whether this is a valid representation of the surface layers. In literature no reference can be found on the optical properties of SiF except for a complex refractive index for a rough SiF layer of $\tilde{n} = 1.6$ determined by Oehrlein.[29] Layadi and coworkers[30] determined a complex refractive index for a SiCl layer of $\tilde{n} = 1.66$, which should be somewhat similar to SiF considering the nature of F and Cl. However, since the reaction layer is known to be just a few monolayers thick,[13] here a first approach will be to consider the contribution of the SiF layer to be negligible in contrast to the surface roughness. Hence, no SiF contribution will be incorporated in the layer models.

B. Results ellipsometry

In Fig. 6, simulations are shown in which the rough layer is assumed to have a certain thickness and the thickness of the underlying *a*-Si layer has been varied (along each thin line). At a given point in time, the measurement matches a

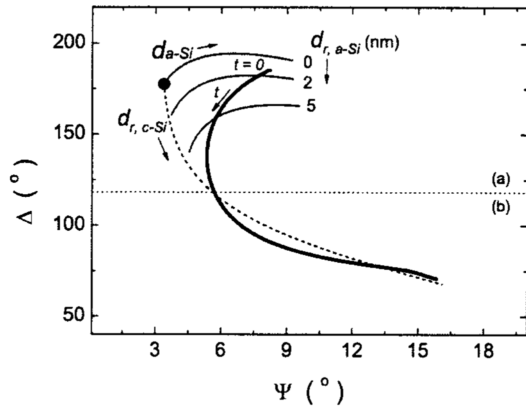

FIG. 6. Ellipsometry trace of the XeF_2 etching of first the *a*-Si layer followed by etching of the underlying *c*-Si bulk (thick line). In region (a) the model in Fig. 5(a) is used (thin line). The rough layer thickness $d_{r,a\text{-Si}}$ is set at a fixed value, whereas the amorphized layer thickness $d_{a\text{-Si}}$ is varied. In region (b) the model in Fig. 5(b) is used (dashed line), which is shown here for a constant void percentage $x=50\%$ (50% void/50% *c*-Si) and a variable rough layer thickness $d_{r,c\text{-Si}}$. By matching the simulations to the measurement the rough layer thickness as a function of time is derived.

specific simulation. In this way, the rough layer thickness and *a*-Si layer thickness can be obtained. Eventually, the *a*-Si is fully removed, leaving only a rough *c*-Si layer on top of the bulk *c*-Si [Fig. 5(b)]. A simulation of this model with a 50% void/50% *c*-Si as a function of rough layer thickness can be seen in Fig. 6 (dashed line). A fair agreement with the long term behavior can already be observed.

In Fig. 7, the measurement (thick line) and simulations for three %void/% *c*-Si ratios are shown as a function of the rough layer thickness $d_{r,c\text{-Si}}$, originating in the point $d_{r,c\text{-Si}}=0$ (dot). For the two cross lines the %void/% *c*-Si ratio has been varied in the range of 20%/80% to 70%/30% for $d_{r,c\text{-Si}}=15$ and 20 nm, respectively. By matching the simulation to the measurement, the rough layer thickness as a function of time can be derived. Note, that for Ψ between 6° and 9°, the measurement comes close to the simulation with a 40% void/60% *c*-Si ratio, then going back to the 50% void/50% *c*-Si simulation. A 40%/60% ratio for %void/% *c*-Si can be seen as a surface that has a cusplike shape as is illustrated in Fig. 8. Such a rough layer can only arise from a process that etches faster in the direction parallel to the etch direction than in the lateral direction, perpendicular to the etch direction.

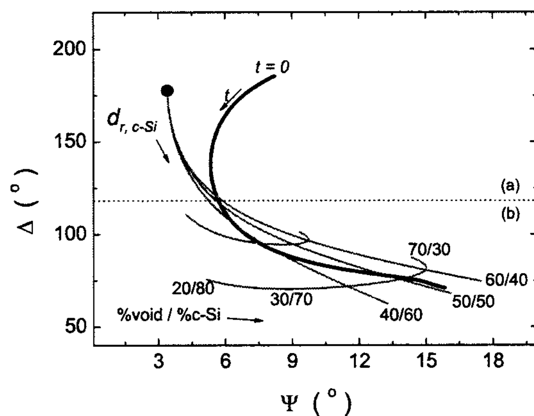

FIG. 7. Simulations and measurement of the long term XeF_2 etching of the *c*-Si bulk resulting from the layer model in Fig. 5(b). For three %void/% *c*-Si ratios the rough layer thickness $d_{r,c\text{-Si}}$ is varied, resulting in the (gray) lines from point $d_{r,c\text{-Si}}=0$ (dot). For the two (gray) cross lines the %void/% *c*-Si ratio has been varied in the range of 20%/80% to 70%/30% for $d_{r,c\text{-Si}}=15$ and 20 nm, respectively. Matching the simulation to the measurement gives $d_{r,c\text{-Si}}$ and the corresponding %void/% *c*-Si ratio as a function of time.

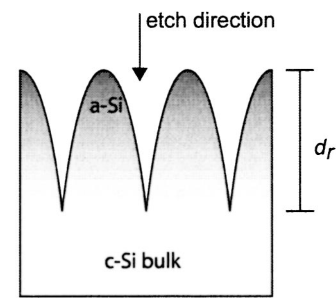

FIG. 8. Representation of a cusplike surface roughness. A lower void percentage in respect to the *c*-Si percentage for the rough layer implies a cusplike shape.

C. Evolution of roughness

The recorded ellipsometry trace in (Ψ,Δ)-space for the XeF_2 etch process in time is shown in Fig. 6 (thick line). At $t=0$ the etch process starts. First both Ψ and Δ decrease as a function of time [region (a)] followed by a region [region (b)] where Ψ increase again but Δ keeps decreasing. In Fig. 9 the results of the analysis of the ellipsometry data as a function of the dose $D(XeF_2)$ of the impinging reactant flux is shown. On the left-hand side, the thickness d_r of the rough layer is shown and on the right-hand side, the measured SiF_4 production coefficient δ is shown. The letters (a) and (b) corresponds to which model from Fig. 5 has been used for curve-fitting the data. Initially, the roughness slowly increases followed by an intermediate phase starting at $D(XeF_2)\approx 2\times 10^3$ ML, in which the roughness shows a rapid increase. Finally, at $D(XeF_2)\approx 1.2\times 10^4$ ML, the roughness increases slow again. In the initial and final phase

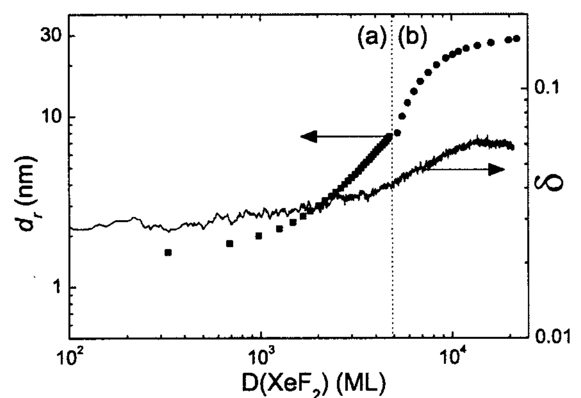

FIG. 9. Rough layer thickness d_r (left axis) and the simultaneously monitored SiF_4 production coëfficient δ (right axis) as function of XeF_2 dose.

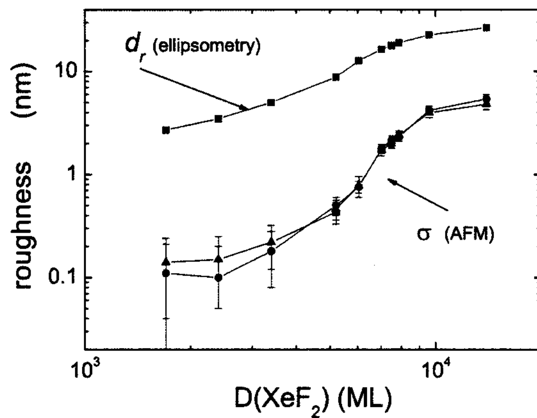

FIG. 10. Roughness as a function of XeF_2 dose in terms of rough layer thickness d_r from ellipsometry and root-mean-square roughness σ from AFM measurements. All samples have been measured twice, resulting in the two series of points

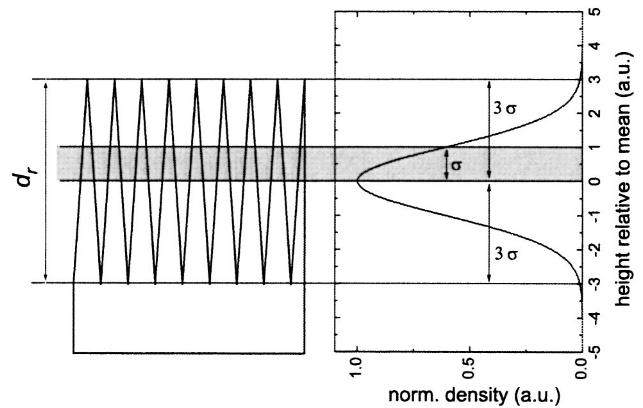

FIG. 11. Representation of rough layer thickness d_r and root-mean-square roughness σ. The AFM measures a distribution of heights relative the mean height. The roughness from AFM measurements is given by the standard deviation or root-mean-square σ of the heights distribution. Ellipsometry measures the total width of the heights distribution d_r. Statistically relevant are the heights between plus and minus 3σ. Therefore, $d_r \approx 6\sigma$.

an increase $d_r \sim D(XeF_2)^{\beta}$ with $\beta \approx 0.2$ is observed, whereas in the intermediate phase a strong anomalous increase is observed, corresponding to $\beta \approx 1.5$. The two completely different models show clearly a convergence, which is a first indication that the models are indeed a good representation of the XeF_2 etch process and that the silicon-fluoride reaction layer can be considered transparent to the ellipsometer.

The production coefficient or etch efficiency δ first shows an increase proportional to $D(XeF_2)^{0.1}$ up to a dose 5×10^3 ML of XeF_2. Next, a switch to an increase $\delta \sim D(XeF_2)^{0.7}$ can be seen, which then levels off at $D(XeF_2) \approx 1.2 \times 10^4$ ML. By etching through the amorphous-to-crystalline transition the total surface area increases significantly. A significantly larger surface area would imply that more sites are available to the incoming etchant. Etch products can be created more easily, hence the etch rate goes up.

D. AFM data

To have an independent measurement of the surface roughness, samples are prepared for various XeF_2 doses and are analyzed *ex situ* with an atomic force microscope (NT-MDT Solver P47) in noncontact mode. Here, the AFM results are compared to the ellipsometry results.

In Fig. 10 both the rough layer thickness from ellipsometry and the roughness σ from the AFM measurements are shown as a function of the XeF_2 dose. Two series of AFM measurements are shown, taken at different positions of the sample with 1×1 μm scan size. Both show a similar trend in roughness evolution. Comparing AFM and ellipsometry measurements is not straightforward since the measure for roughness is defined differently for both diagnostics. The root-mean-square roughness σ (or interface width w) measured by AFM is the standard deviation of the heights measured in the rough layer, whereas ellipsometry measures the total thickness of the rough layer d_r. An illustration of the two measures is shown in Fig. 11.

Here, d_r is assumed twice the 3σ interval of heights distribution, hence

$$d_r \approx 6\sigma. \tag{6}$$

This definition is based on the statistical statement that a height data point outside the 3σ interval is most probably erroneous.[31] This way the statistically relevant part of the height distribution function is taken into account. Thus, by plotting the rough layer thickness against the corresponding root-mean-square roughness σ a comparison on basis of Eq. (6) can be made (Fig. 12).

The comparison seems valid for the long dosed samples. However, at short-term and mid-term (*a*-Si to *c*-Si transition) the measurements show $d_r \gg 6\sigma$. This is related to the way

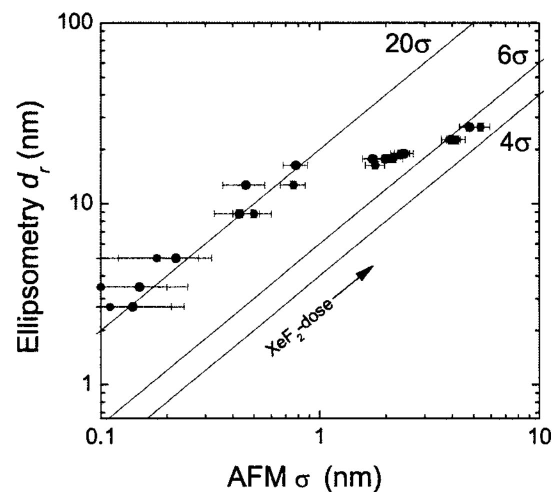

FIG. 12. Rough layer thickness d_r from ellipsometry as a function of the corresponding root-mean-square roughness σ from AFM measurements. Lines with d_r=20σ, 6σ, and 4σ are shown. As a consequence of AFM tip size ξ_{tip}, defined in Fig. 13, the σ is an underestimation of the roughness, thus $d_r \leq 20\sigma$. In the long term limit the AFM tip size is small compared to the surface roughness; $d_r \approx 6\sigma$ is a good quantitative comparison between ellipsometry and AFM. Note that d_r remains well above the 4σ line.

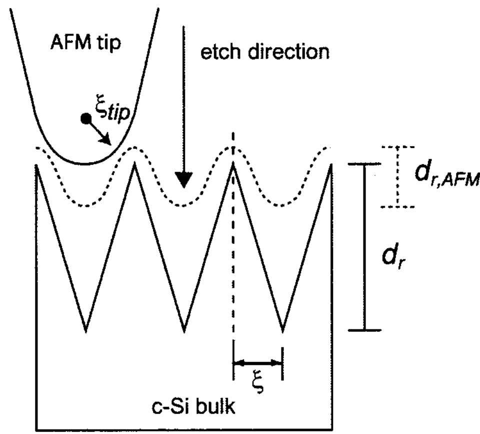

FIG. 13. Underestimation of the roughness occurs when AFM tip radius $\xi_{\rm tip}$ is larger or on the order of lateral dimension ξ and $\xi < d_r$. Consequently the sampled roughness $d_{r,\rm AFM}$ is smaller than the real roughness d_r.

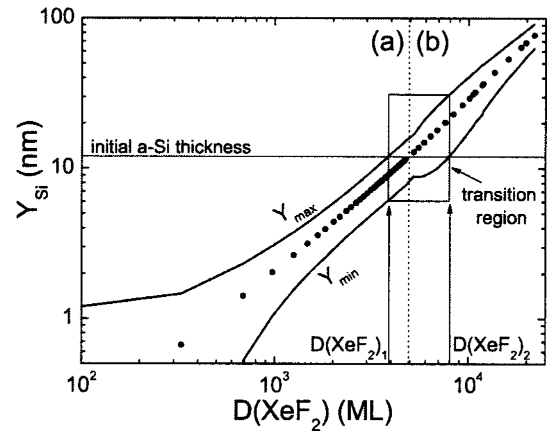

FIG. 14. Si etch yield $Y_{\rm Si}$ as a function of XeF_2 dose $D(XeF_2)$ (●). The lines $Y_{\max}=Y_{\rm Si}+d_r/2$ and $Y_{\min}=Y_{\rm Si}-d_r/2$ cross the initial *a*-Si layer thickness at $D(XeF_2)_1$ and $D(XeF_2)_2$, respectively. These boundaries define the *a*-Si to *c*-Si transition region.

the roughness develops. If the roughness develops more rapidly in etch direction but lateral dimension ξ stays smaller or is on the order of the AFM tip radius ($\xi_{\rm tip}=10$ nm), the AFM is not able to sample the surface properly (Fig. 13). The consequence is an underestimation of the roughness obtained with the AFM. In the long term, the lateral dimension ξ grows and becomes larger than the AFM tip radius $\xi_{\rm tip}$, which results in a proper sampling of the surface by AFM, hence the comparison on basis of Eq. (6) shows good agreement with the experiments. In addition, a $d_r \cong 4\sigma$ comparison line is added, which merely illustrates how sensitive is the comparison on the basis of Eq. (6).

E. Anomalous roughening

All independent diagnostics for the surface roughness, i.e., the ellipsometry data, the AFM data and the etch efficiency show anomalous behavior roughly centered at the transition from the *a*-Si top-layer to the *c*-Si bulk. Here, an attempt is done to qualitatively explain this behavior. First, a simple plot to define the extent of the transition region is introduced. The average thickness of the layer removed by etching is given by the integral version of Eq. (5), equal to

$$Y_{\rm Si}(t)=\frac{1}{2}a_{\rm Si}\int_0^t \delta(t')\Phi_s(XeF_2)dt' \quad (7)$$

where $t' = D(XeF_2;t')/\Phi_s(XeF_2)$.

In Fig. 14 the Si etch yield $Y_{\rm Si}$ is shown as a function of $D(XeF_2)$ for easy comparison with our earlier plots. Additionally, plots of the functions $Y_{\max}=Y_{\rm Si}+d_r/2$ and $Y_{\min}=Y_{\rm Si}-d_r/2$, which represent the upper and lower bounds of the structures on the roughened surface. The dose (or point in etching time) where $Y_{\max}=12$ nm, the thickness of the *a*-Si layer at $t=0$, represents the time where the first *c*-Si patches start to become "visible" to the reactant. Conversely, the dose where $Y_{\min}=12$ nm, determines the point in time where the last cap of *a*-Si disappears from the sample. These two values $D(XeF_2)_1=4\times10^3$ ML and $D(XeF_2)_2=8\times10^3$ ML determine the region where both *a*-Si and *c*-Si have to be considered, the transition region. The anomalous behavior of roughening is contained in this transition region. In this region the shape of the structures, i.e., the surface morphology, changes.

To conclude, in the analysis of the ellipsometry data with model Fig. 5(b) in this transition region the best description is obtained for a 40% void/60% *c*-Si ratio, while a 50%/50% ratio is relevant for the final phase of pure *c*-Si etching for $D(XeF_2)>1.2\times10^4$ ML. This suggests a cusplike shape of the pits in the surface in the transition region. Both features suggest that the remaining *a*-Si patches on the surface effectively act as a capping layer which causes the growth of deep and narrow trenches in the bulk *c*-Si. As a result the number of surface sites, i.e., the total surface area, increases. More sites are available to the incoming etching and, hence, the etch rate increases. The ellipsometry data on the roughness are corroborated by the AFM data, where in this transition region the measured variation σ of the height distribution function is way too small as compared to the thickness d_r. This again suggests narrow and deep surface pits that cannot be tracked by the AFM tip in the transition region. Figure 15 illustrates the full etch process in the three phases.

V. ROUGHNESS IN REACTION LAYER MODELS

A severe surface area increase will have consequences for the kinetic reaction dynamics models that have been proposed in the past. Some issues concerning the reaction layer during XeF_2 etching, such as the "real" or local reaction layer thickness, are still open for debate, hence a discussion in the following section is an attempt to explain the local reaction layer thickness on basis of surface area increase due to roughening.

The local reaction layer thickness is the reaction layer thickness at the atomic scale, which is the parameter of most interest. However, when the surface area increases significantly, the reaction layer thickness obtained with almost all diagnostics tools is an area-integrated layer thickness. There-

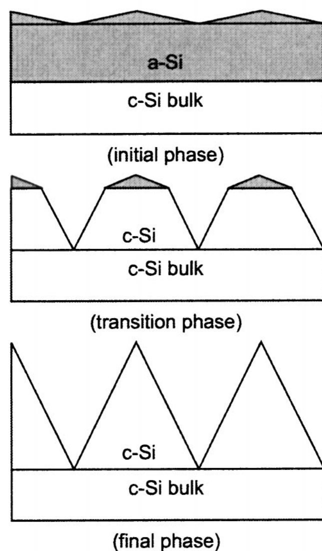

FIG. 15. Initial (a), transition (b), and final (c) phase of the XeF_2 etch process.

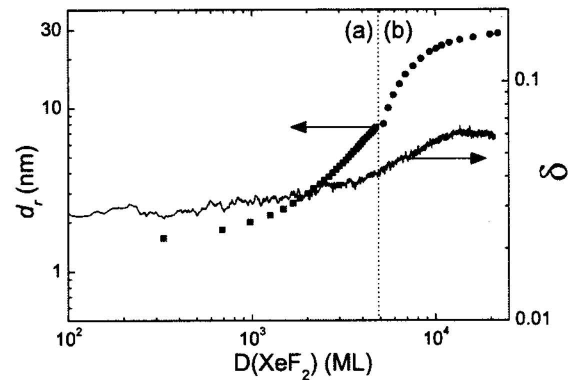

FIG. 16. Surface area increase ρ, $SiF_{1,2}$, and SiF_3 surface coverage (in ML) and SiF_4 production coëfficient $\delta_{\rm calculated}$ resulting from the bilayer model, as well as the measured $\delta_{\rm measured}$, as a function of XeF_2. For a XeF_2 dose less than 10^3 ML, ρ is equal to 1 and the SiF_x coverages follow from matching $\delta_{\rm calculated}$ with $\delta_{\rm measured}$ by determining the back bond breaking probability k_b and etching probability k_e. For XeF_2 dose above 10^3 ML, the increase ρ in surface area is the only variable used to match $\delta_{\rm calculated}$ with $\delta_{\rm measured}$.

fore, this measure is no longer equal to the local reaction layer thickness $d_{\rm local}$, but is an effective reaction layer thickness $d_{\rm eff}$,

$$d_{\rm eff} = \rho d_{\rm local}, \tag{8}$$

where ρ is the ratio of the area along the ragged peaks and valleys of the rough surface as compared to the effective area by looking at the bulk of the sample. Thus ρ is the relative increase in available surface sites due to the roughening.

Some experiments in the past have lead to the interpretation that the SiF reaction layer should be several monolayers (up to 10 ML) thick in order to explain the observations.[2] However, Lo *et al.*[13] concluded from x-ray photoemission spectroscopy (XPS) measurements that the SiF layer thickness is only 1.7 ML and the observed thick reaction layer is a consequence of surface roughness and not as suggested due to fluorine diffusion into the silicon.[2] Vugts *et al.* arrived at the same conclusion by estimating the roughness on the basis of accurate (TDS) measurements with a mass spectrometer.[7] In this article, the surface roughness has been characterized; all information is present to review the available reaction layer models.

A simple but adequate model for XeF_2 etching of Si, the bilayer model,[7,13] is used here for the discussion. A fast fluorination of Si–Si* surface sites results in Si–SiF and Si–SiF_2 species. Next the Si–Si back bonds are broken, leading to SiF_3 species at the surface. Then, the last bond can be broken leading to SiF_4 etch products. Basically, a simple description to visualize the reaction layer is a subsurface monolayer of SiF and SiF_2 species (partially) covered by a layer of SiF_3 species. The rate equations for the bilayer model are as follows:

$$\frac{\partial[\mathrm{SiF}_{1,2}]}{\partial t} = k_f \Phi_s(\mathrm{XeF}_2)\left(1 - \frac{[\mathrm{SiF}_{1,2}]}{\rho N_0}\right) \tag{9}$$

$$\frac{\partial[\mathrm{SiF}_3]}{\partial t} = k_b \Phi_s(\mathrm{XeF}_2)\left(\frac{[\mathrm{SiF}_{1,2}]}{\rho N_0} - \frac{[\mathrm{SiF}_3]}{\rho N_0}\right) - k_e \Phi_s(\mathrm{XeF}_2)\left(\frac{[\mathrm{SiF}_3]}{\rho N_0}\right), \tag{10}$$

in which k_f is the fluorination probability, k_b is the back-bond breaking probability and k_e the etch probability. Here, $[SiF_{1,2}]$ and $[SiF_3]$ are the surface concentrations of the corresponding species in ML on a flat surface. The parameter N_0 is the Si surface concentration for a flat surface (ρ=1, N_0 =1 ML). The formation of etch products is expressed in δ as

$$\delta = 2k_e[\mathrm{SiF}_3], \tag{11}$$

which has already been shown in Fig. 9. With the proper parameter values for ρ, k_f, k_b, k_e, and N_0, the value of δ can be calculated and fitted to the measured δ. In Fig. 16 again δ is shown as a function of XeF_2 dose, together with ρ and coverage of $SiF_{1,2}$ and SiF_3 species (ML).

A discrimination is made between short-term and long-term parameter values. The bilayer model simulations are obtained as follows. For a XeF_2 dose below 10^3 ML (=short term) the surface area increase ρ is assumed to be close to 1. The true reaction layer growth can be observed. The $SiF_{1,2}$ species first start to generate a monolayer coverage. This layer gets covered for about 50% by SiF_3 species leading to the steady state reaction layer. To perform the simulations, k_f is taken from Vugts *et al.*,[7] ρ and N_0 are fixed, whereas k_b and k_e are used to fit the calculated δ to the measured δ. The fixed and fitted parameter values are listed in Table II. For a XeF_2 dose above 10^3 ML due to the etch process the roughness increases, which results in an increase of the surface area. Therefore, k_f, k_b, k_e, and N_0 are kept fixed to their values derived from the short term fit to the measured δ. Only ρ is used to fit the increase in the measured δ. The concentration of $SiF_{1,2}$ species grows with the same factor as the surface area increase, thus also more sites are available to harbor SiF_3 species. Hence, more SiF_3 species

TABLE II. Bilayer model parameters used for short term and long term simulations, including the indication whether the parameter is used as fit parameter or as fixed value.

Parameter	Short term values	Long term values
k_f	0.03 (fixed)[a]	0.03 (fixed)[a]
k_b	0.03 (fit)	0.03 (fixed)
k_e	0.03 (fit)	0.03 (fixed)
N_0	1 ML (fixed)	1 ML (fixed)
ρ	1 (fixed)	var. (fit)
$\Phi_s(XeF_2)$	0.9 ML s^{-1}	0.9 ML s^{-1}

[a]From Reference 7.

are available for SiF_4 etch product formation, which translates into an increase in δ. The increase in δ implies a factor of two increase in surface area. The corresponding $[SiF_{1,2}]$ is in this case about 2 ML with still a 50% SiF_3 coverage: $[SiF_3]=1$ ML. The local reaction layer thickness is 1.5 ML, but the effective thickness is 3.0 ML, if one assumes that the stoichiometry of 1 ML SiF layer to be equivalent to SiF_2 coverage. The local reaction layer thickness of 1.5 ML is in very good agreement with the 1.7 ML reported by Lo *et al.*,[13] who used XPS to measure the local reaction layer thickness. It also shows that the effective layer thickness is twice the local reaction layer thickness, since the surface area has increased with a factor of two.

The effective thickness is basically the measure usually reported in literature, because almost every diagnostic gives the area integrated layer thickness instead of the local layer thickness. It is therefore questionable whether the assumption made by various authors that a rather thick reaction layer is created in the etch process due to fluorine diffusion, is in fact a 1.5 ML thick reaction layer stretched out along a rugged and rough surface profile. Thus, the assumption that the SiF-layer contribution to the ellipsometry measurement can be considered negligibly small is valid. Even when the effective layer thickness becomes 3 ML, the roughness is such that the SiF-layer contribution is much smaller than the surface roughness. It should be noted that the roughening, thus also surface area increase, may be related to experimental conditions such as Si crystal orientation, doping level, etchant nature (XeF_2, F_2, F, Cl_2, Cl) and flux, sample history, and maybe many more experimental parameters. The reported SiF reaction layer of several monolayers (up to 10 ML) thick in past observations[2] may well be explained by an increase in surface area, depending on the specific experimental conditions.

VI. SURFACE MORPHOLOGY

With the rough layer thickness d_r obtained from ellipsometry and the surface area increase ρ obtained from the product coëfficient δ, a detailed description of the surface morphology can be derived. A three-dimensional geometric representation for the rough layer is required. The chosen geometry is a repetitive pattern [Fig. 17(a)] of the unit cell, which is constructed of a pyramid pointing upwards and a

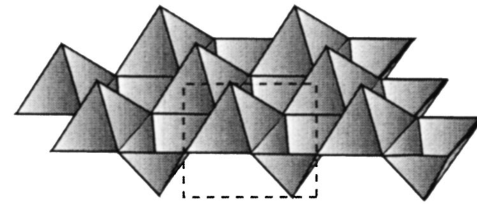

(a) 3-D geometry

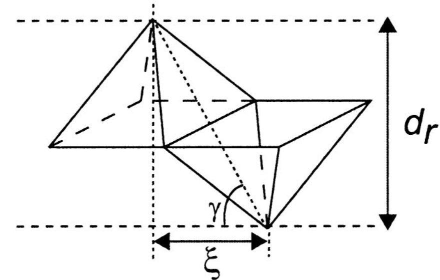

(b) unit cell

FIG. 17. Geometrical model for the rough layer (a) and corresponding unit cell (b). The rough layer thickness d_r is the peak–to–peak height difference and ξ is the peak–to–peak lateral dimension. The average surface-slope angle is the angle γ as defined in (b).

pyramid pointing downwards [Fig. 17(b)]. Now, the surface area increase ρ can be geometrically calculated by

$$\rho=\sqrt{1+\frac{d_r^2}{\xi^2}}, \tag{12}$$

in which d_r is the peak-to-peak height difference. Dimension ξ equals the peak-to-peak lateral dimension. Actually, this formula is valid for both the three-dimensional and two-dimensional cases. Thus, the lateral dimension ξ here is equal to ξ defined in Fig. 13. Since ρ and d_r have been experimentally determined the lateral dimension ξ can be calculated.

At the beginning of the transition $[D(XeF_2)_1=4\times10^3$ ML, Fig. 14] ξ is found to be equal to 6.6 nm with d_r=5.9 nm and at the end of the transition $[D(XeF_2)_2=8\times10^3$ ML, Fig. 14] ξ=12.9 nm with d_r=18.7 nm. In the transition phase ξ becomes smaller than d_r and is smaller than the AFM tip radius ξ_{tip}=10 nm. Again this substantiates the fact that this type of surface roughness cannot be properly tracked with the AFM. In the final phase at $D(XeF_2)=2\times10^4$ ML, the value of ξ is found to be 15 nm with d_r=27.8 nm. Here, ξ is significantly larger than the ξ_{tip}, hence the roughness can be tracked properly.

Now, the average surface-slope angle can be determined, as given by the angle γ as defined in Fig. 17(b). For $D(XeF_2)=2\times10^4$ ML the angle is found to be 62°. At 54° with respect to the Si(100) crystal plane lies the Si(111) plane, which is close to the 62° that is found here. This suggests that the roughness growth in the final phase has

arrived at a steady state, i.e., surface area increase remains constant, which is governed by the etching of the Si(111) plane.

VII. CONCLUSIONS

Single wavelength ellipsometry has been successfully employed to characterize the surface roughness caused by physical Ar^+ etching and chemical XeF_2 etching. The proposed ellipsometry layer models give a good representation of the etch process. Preliminary results with spectroscopic ellipsometry show a similar behavior. Thus, for the $Ar^+/XeF_2/c$-Si system single wavelength ellipsometry has proven to be a good tool to monitor surface roughness. For XeF_2 etching of the *a*-Si layer and subsequently the *c*-Si bulk sample, the roughness evolution shows an anomalous roughening. When etching through the amorphous to crystalline transition the roughness increases proportional to $D(XeF_2)^{1.5}$ and, simultaneously, the etch rate shows an increase. Since etching is faster in the direction parallel to the etch direction than in the lateral direction, the surface shows a cusplike shape and hence the surface area increases severely. Presently, studies are devoted to answer the question why the etching goes faster in the etch direction as opposed to the lateral direction. In the *a*-Si to *c*-Si transition region the remaining *a*-Si patches act as a capping layer, which might suggest an etch rate difference between *a*-Si and selected crystal faces of *c*-Si. A comparison with AFM measurements substantiates the anomalous roughening. On the basis of the bilayer model for XeF_2 etching of silicon an estimation of the surface area increase yields an increase of a factor of 2. The resulting local reaction-layer thickness of 1.5 ML is in agreement with the 1.7 ML reported by Lo *et al.*[13] Such a thin SiF reaction layer can be considered transparent to the ellipsometer and can therefore be disregarded in the ellipsometry layer models. Due to surface area increase this SiF layer becomes effectively 3 ML, but this is still negligibly small in comparison to the roughness. These separate studies of Ar^+ and XeF_2 etching will facilitate a basis for studying the surface roughness caused by the Ar^+ ion assisted XeF_2 beam etching of silicon.

ACKNOWLEDGMENTS

The authors wish to acknowledge J. A. C. M. v.d. Ven and L. H. A. M. v. Moll for the technical support and W.M.M. Kessels and M. C. M. v.d. Sanden for the supporting discussions. This research is supported by The Netherlands Foundation for Fundamental Research on Matter (FOM: 99TF24).

[1] J. W. Coburn and H. F. Winters, J. Appl. Phys. **50**, 3189 (1979).
[2] J. W. Coburn and H. F. Winters, Surf. Sci. Rep. **14**, 161 (1992).
[3] G. J. P. Joosten, M. J. M. Vugts, H. J. Spruijt, H. A. J. Senhorst, and H. C. W. Beijerinck, J. Vac. Sci. Technol. A **12**, 636 (1994).
[4] M. J. M. Vugts, G. J. P. Joosten, A. van Oosterum, H. A. J. Senhorst, and H. C. W. Beijerinck, J. Vac. Sci. Technol. A **12**, 2999 (1994).
[5] M. J. M. Vugts, L. J. F. Hermans, and H. C. W. Beijerinck, J. Vac. Sci. Technol. A **14**, 2138 (1996).
[6] M. J. M. Vugts, G. L. J. Verschueren, M. F. A. Eurlings, L. J. F. Hermans, and H. C. W. Beijerinck, J. Vac. Sci. Technol. A **14**, 2766 (1996).
[7] M. J. M. Vugts, M. F. A. Eurlings, L. J. F. Hermans, and H. C. W. Beijerinck, J. Vac. Sci. Technol. A **14**, 2780 (1996).
[8] M. J. M. Vugts, L. J. F. Hermans, and H. C. W. Beijerinck, J. Vac. Sci. Technol. A **14**, 2820 (1996).
[9] P. G. M. Sebel, L. J. F. Hermans, and H. C. W. Beijerinck, J. Vac. Sci. Technol. A **17**, 755 (1999).
[10] P. G. M. Sebel, L. J. F. Hermans, and H. C. W. Beijerinck, J. Vac. Sci. Technol. A **17**, 3368 (1999).
[11] P. G. M. Sebel, L. J. F. Hermans, and H. C. W. Beijerinck, J. Vac. Sci. Technol. A **18**, 2090 (2000).
[12] P. G. M. Sebel, L. J. F. Hermans, and H. C. W. Beijerinck, J. Vac. Sci. Technol. A **18**, 2759 (2000).
[13] C. W. Lo, D. K. Shuh, V. Chakarian, T. D. Durbin, P. R. Varekamp, and J. A. Yarmoff, Phys. Rev. B **47**, 648 (1993).
[14] V. S. Aliev, V. N. Kruchinin, Surf. Sci. **442**, 206 (1999).
[15] M. Fried, T. Lohner, E. Jároli, Gy. Vizkelethy, G. Mezey, J. Gyulai, M. Somogyi, and H. Kerkow, Thin Solid Films **116**, 191 (1981).
[16] J. L. Buckner, D. J. Vitkavage, E. A. Irene, and T. M. Mayer, J. Electrochem. Soc. **133**, 1729 (1986).
[17] J. F. Ziegler, J. P. Biersack, and U. Littmark, *The Stopping Range of Ions in Solids* (Pergamon, Oxford, 1985).
[18] D. B. Graves, D. Humbird, Appl. Surf. Sci. **192**, 72 (2002).
[19] R. Pétri, P. Brault, O. Vatel, D. Henry, E. André, P. Dumas, and F. Salvan, J. Appl. Phys. **75**, 7498 (1994).
[20] A. C.-T. Chan, G.-C. Wang, Surf. Sci. **414**, 17 (1998).
[21] J. G. C. Labanda, S. A. Barnett, L. Hultman, J. Vac. Sci. Technol. B **16**, 1885 (1998).
[22] R. M. A. Azzam and N. M. Bashara, *Ellipsometry and Polarized Light* (North-Holland, Amsterdam, 1992).
[23] D. A. G. Bruggeman, Ann. Phys. (Leipzig) **24**, 636 (1935).
[24] G. M. W. Kroesen, G. S. Oehrlein, E. de Frésart, and M. Haverlag, J. Appl. Phys. **73**, 8017 (1993).
[25] A. H. M. Smets, D. C. Schram, and M. C. M. van de Sanden, J. Appl. Phys. **88**, 6388 (2000).
[26] A. A. E. Stevens and H. C. W. Beijerinck (unpublished).
[27] C. Casiragh, A. C. Ferrari, R. Ohr, A. J. Flewitt, D. P. Chu, and J. Robertson, Phys. Rev. Lett. **91**, 226104 (2003).
[28] Dae Won Moon and Kyung Joong Kim, J. Vac. Sci. Technol. A **14**, 2744 (1996).
[29] G. S. Oehrlein, J. Vac. Sci. Technol. A **11**, 34 (1993).
[30] N. Layadi, V. M. Donnely, J. T. C. Lee, and F. P. Klemens, J. Vac. Sci. Technol. A **15**, 604 (1997).
[31] H. M. Wadsworth Jr., *Handbook of Statistical Methods for Engineers and Scientists* (McGraw-Hill, London, 1990).
[32] *Handbook of Optical Constants of Solids*, edited by E. D. Palik (Academic, London, 1998), Vol. I, pp. 547–569.
[33] *Handbook of Optical Constants of Solids*, edited by E. D. Palik (Academic, London, 1998), Vol. I, pp. 749–736.